Molecular dynamics simulation of thin film growth on giant magnetoresistance corrugated structures

Cheng-I Weng*
Department of Mechanical Engineering, National Cheng Kung University, Tainan, Taiwan, Republic of China

Chi-Chuan Hwang†
Department of Engineering Science, National Cheng Kung University, Tainan, Taiwan, Republic of China

Chia-Lin Chang, Jee-Gong Chang,‡ and Shin-Pon Ju
Department of Mechanical Engineering, National Cheng Kung University, Tainan, Taiwan, Republic of China

(Received 16 July 2001; revised manuscript received 9 January 2002; published 10 May 2002)

This paper presents the use of molecular dynamics (MD) in simulating thin-film growth on giant magnetoresistance corrugated structures. The simulation model mainly concerns the deposition of Co atoms on a *V*-shape Cu substrate. The many-body, tight-binding potential model is utilized in the MD simulation to represent the interatomic force that exists between the atoms. The interface width is used to quantify the variation of surface roughness at the transient and steady states. The paper investigates the influence of incident energy on the deposited film surface property and on the growing mechanism, for both vertical and oblique deposition. The results demonstrate how the growing characteristics are influenced by different incident energies and by different deposition directions. It is found that at relatively low incident energies the film growth tends to be in a three-dimensional cluster mode and that a void track is formed, whose growing direction is almost equal to the surface normal to the two inclined surfaces. The uneven thickness found along the base of the *V* shape is mainly due to the deposited atoms that accumulate at the bottom of the *V* groove when the incident energy is at a relatively high level. It is found that there exists an optimal incident energy that produces the best film surface property. The film surface property can be improved by changing the incident direction relative to the two inclined directions of $\pm 45°$. Smaller deviation angles yield better film surface properties for low incident energy. Conversely, higher levels of incident energy result in worse film surface properties.

DOI: 10.1103/PhysRevB.65.195420 PACS number(s): 81.07.−b, 83.10.Rs, 73.43.Qt, 52.65.Yy

I. INTRODUCTION

Giant magnetoresistance (GMR) material has been widely used in many applications, such as magnetic storage systems[1–4] and microsensors.[5,6] In order to meet the increasingly rigorous requirements that are demanded in practice, much effort has been devoted to improving the magnetoresistance (MR) properties of thin magnetic films and multilayers by pattering the multilayer into either a column[7] or into a corrugated structure.[8] The advance of fabrication technology for semiconductors, together with the ongoing attempts to apply new fabrication technologies to the manufacture of magnetic devices, has resulted in a dramatic reduction in the size of such devices. This has made possible new applications of magnetic devices at the microscale and nanoscale, such as magneto-optic recording systems[9,10] and magnetic quantum devices.[11] However, the practical fabrication difficulties encountered also increase due to the abrupt increase in the surface area to volume ratio of the device. In devices of this scale, surface defects and poor surface roughness cannot be tolerated since they fatally affect the MR property of the deposited film.

It has been reported in former literature that the surface roughness of the deposited film influences its MR property. Fullerton *et al.*[12] concluded that higher interfacial roughness is beneficial for the MR property. However, Ueda *et al.*[13] stated that the MR property is better when the interfacial roughness is lower. It would appear, therefore, that the relationship between the GMR property and the structural properties,[14] including the interfacial roughness between Co/Cu multilayers, and the surface roughness of the Si substrate, has not yet been fully understood.[15] Different fabrication technologies that produce good quality film with a larger MR ratio on a Co/Cu multilayer structure have been suggested. These include ion-beam sputtering,[16] dc magnetron sputtering,[17] oblique deposition,[18] and vertical deposition[8] techniques. Very little is known about the growing mechanisms of deposited surface films and the relationship between the growing modes and the process parameters for different process techniques. An understanding of this relationship is essential if the desired film properties, which are strongly connected to the final film roughness, are to be achieved by controlling the process parameters.

The small size of the features involved means that it is very difficult to observe film growth in the transient state during real experiments, and therefore it is difficult to obtain a complete understanding of the growing mechanism from experimentation alone. As a consequence, the understanding of film growth mechanisms must be investigated with the aid of simulation methods, such as the Monte Carlo method,[19] and MD simulation. Although MD simulation has been used before to study the growing mechanism of film deposition, most of the research has been restricted to the case of vertical deposition on a flat substrate.[20–23] Since vertical deposition for a GMR corrugated structure (see Fig. 1) is equivalent to oblique deposition for a flat substrate, the conclusions concerning growing mechanisms, which have been drawn from former studies of vertical deposition on a flat substrate can-

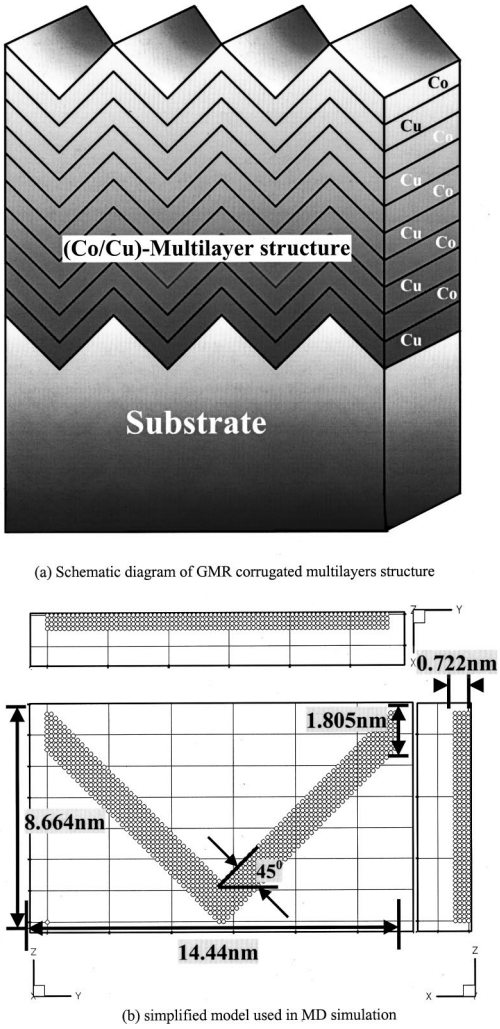

FIG. 1. (a) Schematic diagram of GMR corrugated multilayers structure and (b) simplified model used in MD simulation.

not be applied directly to vertical deposition on a GMR corrugated structure. Dong *et al.*[24] used two-dimensional MD simulation to investigate the influence of process parameters, including incident energy and substrate temperature on the film microstructure of an oblique deposition. The pairwise, Lennard-Jones potential method was employed to simulate the atomic force among the deposited atoms, as well as the substrate atoms. They concluded that void formation, alignment into tracks, and the columnar structure are all attributable to the shadowing effect. They also examined the empirical ''tangent law,'' which defines the relationship between the deposition angle and the angle of orientation of the columnar tracks. Zhou *et al.*[25] also used two-dimensional MD simulation to investigate vacancy concentration with three working parameters, namely, substrate temperature, incident energy, and incident angle. Ju *et al.*[26] employed the pairwise, Morse potential to investigate the influence of process parameters on film roughness. Their study adopted a three-dimensional model, and focused upon oblique deposition for varying incident angles. They found that a rougher surface is produced as the incident angle increases. Zhou and Wadley[27] used three-dimensional MD simulation to investigate the effects of incident angles, with a special emphasis on atomic reflection and resputtering. They analyzed surface damage, but did not consider film structures. While these studies relating to oblique deposition were useful in providing a deep insight into the growing mechanism during the deposition process, the growing mechanism of film deposited on a GMR corrugated structure is different from that of a film deposited on a flat substrate since the shape of a GMR structure (a *V* shape) is obviously different from that of a flat substrate. The GMR corrugated structure consists of many grooves etched on the substrate, as seen in Fig. 1.

Fairly recently, the many-body, tight-binding potential model has been derived, which considers the long-range force acting among atoms.[28,29] In contrast to the pairwise potential model, the many-body potential method considers that the interaction between two atoms depends on the local environment around the atoms as well as just the two atoms themselves. The advantages provided by this method are that the Cauchy discrepancy of the elastic constant is well satisfied, and that the surface relaxation, adatom diffusion can be appropriately modeled.[30,31] It has been proven that this method is the equal of other many-body potential approaches, such as the embedded atom method (EAM). In fact, some material properties obtained using this method are superior to those obtained with pairwise potential methods.[28] Moreover, its calculation methodology is straightforward.

Molecular dynamics is employed to simulate thin-film growth on a GMR corrugated structure. The simulation model mainly considers the deposition of Co atoms on the *V*-shape Cu substrate. The many-body, tight-binding potentials approach is utilized in the MD simulation to model the interatomic force between the atoms. The interface width is used to quantify the variation of surface roughness at both the transient and the steady state. The influence of incident energy on the deposited film surface property and on the growing mechanism is investigated for both vertical and oblique deposition. Finally, the paper discusses the impact of different angle distributions on the deposited film property, where these distributions are controlled by defined process parameters, namely, cutoff angle and deviation angle.

II. SIMULATION MODEL

The simulation model consists of four parts: the MD model of the Cu substrate of a corrugated structure, the sputter deposition model, the atomic interaction model of Cu-Co, and the roughness calculation.

The schematic diagram of a GMR corrugated multilayer structure and the corresponding simplified model used in the MD simulation are shown in Figs. 1(a) and 1(b), respectively. In practice, the GMR corrugated structure is fabricated by etching many faceted grooves on a (Si) substrate. As may be seen in Fig. 1(a), the multilayer structure comprises alternate layers of Co and Cu. A three-dimension model is adopted to simulate thin-film growth on the corrugated structure. A basic assumption of the simulation model is that a Cu film has been perfectly grown on the Co substrate. As a consequence, the simulation starts with Co atoms

TABLE I. Parameters used in tight-binding potential.

Parameters	A (eV)	ξ (eV)	p	q	r_0 (Å)
Cu	0.0855	1.224	10.960	2.278	2.556
Co	0.0950	1.488	11.604	2.286	2.502
Co-Cu	0.0900	1.330	11.282	2.282	2.540

deposited on an already grown Cu film, as a substrate. The periodic boundary conditions are applied in the y and x (depth) directions by considering the repeating characteristics of the geometry. In this way, the simulation domain contains only one single groove.

The three lowest layers of the Cu substrate, henceforth referred to as the thermal layer, are used to control the thermal state of the substrate. To be more specific, the scaling method is employed to maintain the thermal layer at a constant temperature. Therefore, the impact energy of the incident Co atoms can be transferred outward through the Cu substrate. Both the Cu substrate and the thermal layer are arranged according to their face-centered cubic (fcc). The Cu substrate and the thermal layer consist of 2770 atoms. The lowest layer is fixed to prevent the substrate atoms from shifting.

The velocity of the individual atoms is given by the following expression:

$$V_{\text{atom}} = \sqrt{\frac{2E_{\text{atom}}}{M}}, \tag{1}$$

where E_{atom} represents the incident energy and M is the atomic mass. The simulation considers two types of deposition methods. These methods are based upon the deposition angle relative to the vertical z direction, and are referred to as vertical deposition and oblique deposition. In practice, the angular distribution is controllable within several deposition processes, e.g. collimated magnetron sputter deposition and ionized magnetron sputter deposition. It is possible to control the angular distribution of the incident atoms such that the distribution lies within a cutoff angle. A rotatable cylindrical magnetron system[32] has recently been developed, which can provide more flexibility in the spatial and angular distributions by adjusting the rotation angle of the two magnetic assemblies. In the simulation, the incident position of the atoms is generated by a random distribution that represents a uniform distribution of atoms over the substrate. The incident angle of the deposited atoms is also generated by a random function, which satisfies the Gaussian distribution. This is to appropriately model the situation that occurs in practice, i.e., the deposited atoms emitted from the target approximately satisfy the cosine angular distribution. In the simulation, the distance between two subsequently deposited atoms is set to be larger than their truncated distance. This is to represent the fact that in practice the atoms rarely interact with each other before reaching the substrate due to the distribution of atoms in a vacuum.

The simulation employs the many-body potential of the tight-binding second moment approximation (TB-SMA) model to represent the interatomic force. The main difference between this model and the between-pair potential model is that it considers the interaction between two atoms to depend on the local environment around the atoms, as well as on the two atoms themselves. The prediction of some properties by the TB-SMA method is more accurate than the EAM method. Furthermore, the computing algorithm used within the TB-SMA method is simpler than the one used by the EAM method. The TB-SMA model commences by summing the band energy, which is characterized by the second moment of the d-band density of state, and a pairwise potential energy of the Born-Mayer type [30], i.e.,

$$E_i = -\left\{ \sum_j \xi^2 \exp\left[-2q\left(\frac{r_{ij}}{r_0} - 1 \right) \right] \right\}^{1/2} + \sum_j A \exp\left[-p\left(\frac{r_{ij}}{r_0} - 1 \right) \right], \tag{2}$$

where ξ is an effective hopping integral, r_{ij} is the distance between atom i and j, and r_0 is the first-neighbor distance. The parameters A, p, q, and ξ are determined by the experimental data of cohesive energy, lattice parameter, bulk modulus, and two shear elastic constants, C_{44} and $C' = 1/2(C_{11} - C_{12})$, respectively. The parameters of the tight-binding potential related to Cu-Cu, Cu-Co, and Co-Co simulated in this study are drawn from Ref. 33 and are listed in Table I. It is to be noted that the cross parameters of Co-Cu are obtained by applying a fitting procedure to a set of experimental enthalpy data relating to the mixing of a liquid alloy.

Finally, the interaction force on atom i can be expressed as

$$\overline{F_i} = \sum_{j \neq i} \left(\frac{\partial E_i}{\partial r_{ij}} + \frac{\partial E_j}{\partial r_{ij}} \right) \frac{\overline{r_{ij}}}{r_{ij}}. \tag{3}$$

The simulation uses the Gear's predictor-corrector algorithm[34] to calculate the trajectories of the atoms. The potential cutoff radius has been extended up to the second neighbor distance for the interactions of Cu-Cu, Co-Co, and Co-Cu in the calculation.

Calculation of the film roughness of the Co deposited in the V-shape substrate is slightly different from the usual case of a film deposited on a flat substrate. The film roughness is calculated along two inclined surfaces that are symmetrical about the vertical axis, as seen in Fig. 1. The interface width R,[35,21,24] is defined as the root-mean-square roughness of the surface atoms on the two inclined surfaces, and is used to quantify the variation of surface roughness. The interface width is given by the following equation:

$$R^2 = \sum_{j=0}^{j=\infty} (Z_j - \overline{Z}_j)^2 N_j, \tag{4}$$

where N_j amounts to the net number of exposed atoms in layer j, and $j=0$ corresponds to the top substrate layer. $\overline{Z}_j$ and Z_j represent the mean height of the film surface and the height of the exposed atoms, respectively. The definition of the interface width given in Eq. (4) allows the calculation to be performed at both the transient state and the steady state.

III. RESULTS AND DISCUSSION

The simulation comprises two parts. The first part investigates the effect of incident energy on the deposited film surface property, while the second part studies the effect of the incident angle on the deposited atoms. For the first part of the simulation, the incident angle is taken as zero degrees relative to the vertical z axis, i.e., vertical deposition. The second part of the simulation focuses upon oblique deposition. The simulation considers two different types of deposition in order to verify the influence of the incident angle on the deposited film surface property. Finally, an assessment is made as to how the surface property of the deposited film may be improved by controlling two defined process parameters, i.e., cutoff angle and deviation angle.

The simulation is terminated when 1400 atoms have been deposited on the substrate, this being equal to 8.7 monolayers. The other parameters adopted in the simulation include a deposition rate of 5 atoms/ps and a substrate temperature of 300 K. These parameters are used throughout the entire simulation, unless noted otherwise.

1. Effect of the incident energy

The morphology of the film growth on the GMR corrugated structure at four different levels of incident energies, i.e., 0.1, 0.5, 3, and 10 eV, is shown in Figs. 2(a)–2(d) at the final steady state. A columnar structure is formed along the two inclined surfaces at the relatively low incident energy of 0.1 eV, as shown in Fig. 2(a). Since the surface free energy of Co (2.709 J m^{-2}) is larger than that of Cu (1.934 J m^{-2}),[36] at relatively low incident energy Co will not readily grow on the Cu substrate in a layer-by-layer growth mode [Frank-ver der Merve (FM) mode]. Its tendency is to grow in a 3D cluster mode [Volmer-Weber (VW) mode] instead. Generally, deposited atoms tend to grow in a FM mode on a substrate with a large number of high-energy broken bonds (higher surface energy) rather than on one with small-energy broken bonds (lower surface energy).

In order to further investigate the growing mechanism of the columnar structure, seven more monolayers are deposited at a constant incident energy of 0.1 eV. Figure 3 shows the final morphology at an instant of 386 ps in the deposition process. From a detailed observation of this growing morphology, it is possible to identify the changes that take place within the void tracks. A comparison of Fig. 3 with Fig. 2(a) shows that some void tracks have been filled by the subsequently deposited atoms. Figure 3 shows that the lowermost

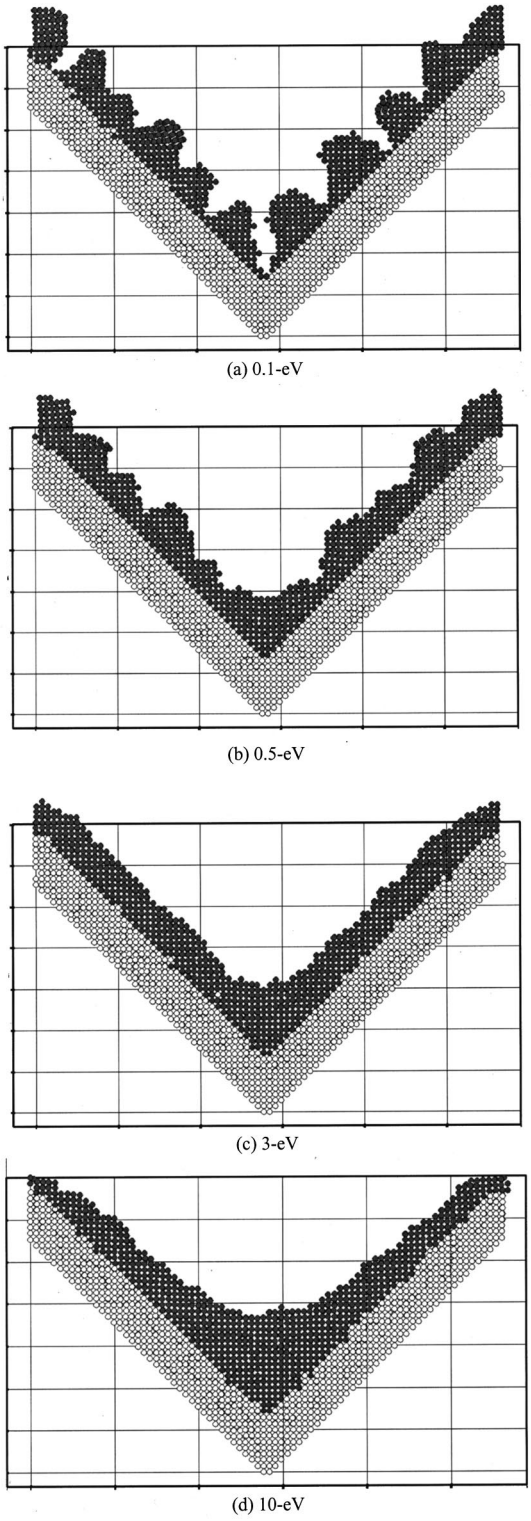

FIG. 2. Morphology of deposited film at final steady state at different incident energies: (a) 0.1 eV; (b) 0.5 eV; (c) 3 eV; (d) 10 eV.

columnar structures on either side of the V shape join at the top, thereby trapping a void within the film at the bottom of the V groove.

Observation of the growing direction of the void tracks

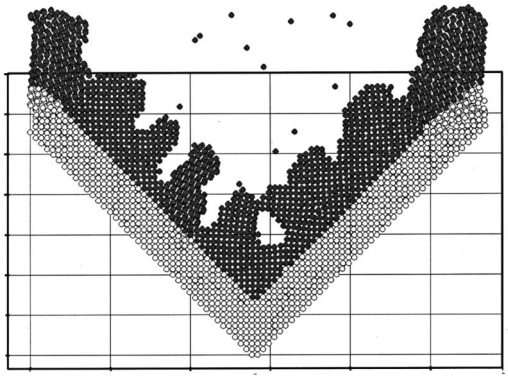

FIG. 3. Snapshots of deposited film morphology at incident energy of 0.1 eV and elapsed time of 380 ps.

evident in Figs. 2(a) and Fig. 3 shows that, apart from one void track grown at the bottom of the *V* groove, the direction of growth appears to be perpendicular to the substrate. This observation is borne out by analysis of snapshots taken at many discrete intervals during the simulation. In a former report, Dong *et al.*[24] concluded that the variation of the column/void track angle, β, with the deposition angle, α, fits well with the tangent law, $\tan\alpha = 2\tan\beta$, at low deposition angles, $\alpha < 60°$. However, examination of Fig. 3 shows no obvious connection between the void track direction and the deposition angle. It will be noted that vertical deposition for a flat substrate corresponds to oblique deposition with an angle of 45° for a *V*-shape substrate. Thus, based upon the conclusions given in Ref. 24, the void tracks direction should be 26° relative to the inclined surface normal. However, the simulation results presented in Fig. 3 show this direction to be approximately zero degrees relative to the inclined surface normal. On other words, this result is inconsistent with that presented by Dong *et al.*[24] This may be explained by the fact that the current simulation considers deposited atoms that are of a different material from the substrate. In the former research,[24] the same material (Ni) is used for both the deposited atoms and the substrate atoms. Therefore, the growing film and the substrate possess the same magnitude of surface energy ($2.0\ \mathrm{J\,m^{-2}}$), and so the growing direction of the void track is mainly influenced by the deposition angle. Since in the current simulation the material of the deposited film and the substrate surface are different, the difference in the magnitudes of the surface energy of the two materials is large. Therefore the deposited Co atoms tend to bond strongly with each other rather than with the Cu substrate atoms. This causes the influence of the deposition direction on the void track forming direction to become insignificant.

Figure 2(b) presents the growing morphology at an incident energy of 0.5 eV. It shows that the void tracks apparent in Fig. 2(a) disappear and are filled by atoms deposited subsequently. This suggests that an increase of incident energy elevates the migration ability of deposited atoms, which is beneficial to the filling of the void tracks. In Ref. 36, it is reported that the self-diffusion activation energy of Co atoms on the fcc Co(100) surface is 0.49 eV. Furthermore, it is reported that a Co fcc structure is chosen as the reference structure because the first few monolayers grown on this surface adopt the same structure configuration as Cu, rather than its original hcp structure observed by reflection high-energy electron diffraction experiments. It seems that the disappearance of the void track at an incident energy of 0.5 eV is strongly connected to the self-diffusion activation energy of the Co atoms on the fcc Co(100) surface. This issue will now be discussed and analyzed further.

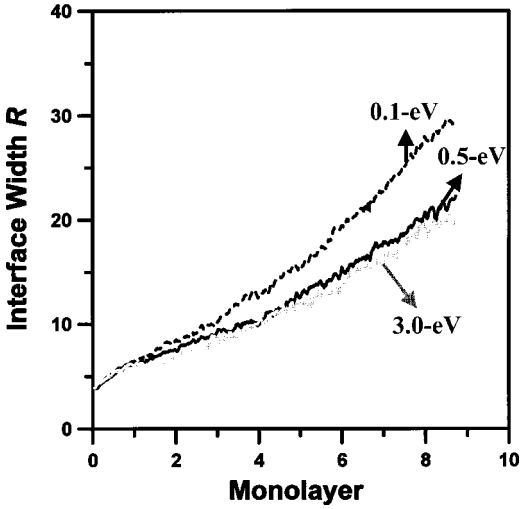

FIG. 4. Transient interface width variation at incident energies of 0.1, 0.5, 3, and 10 eV.

Figure 4 shows the transient interface width for three different levels of incident energy, i.e., 0.1, 0.5, and 3 eV. A close observation of the interface width variation for an incident energy of 0.5 eV shows that the growing behavior of the deposited film on the substrate deviates more from the FM growth mode as more Co atoms have deposited on the substrate. This is demonstrated by the fact that the growing morphology deteriorates after four monolayers have been grown on the Cu substrate, i.e., a slightly higher rate of interface width growth is observed after approximately four monolayers have been grown on the substrate. The physical explanation for this phenomenon can be deduced from the experimental observations reported in Ref. 36. It was noted that the growing structure of the Co atoms deposited on the Cu substrate would gradually depart from the Cu fcc structure. This causes the energy barrier to exceed 0.49 eV. As a consequence, an incident energy of 0.5 eV is insufficient to overcome the energy barrier, and so FM mode film growth for subsequently deposited atoms is hindered.

Referring once again to Fig. 4, it will be observed that the transient interface width greatly decreases when the incident energy increases from 0.1 to 0.5 eV. This improvement in the film surface property is greater than the improvement noted when the incident energy increases from 0.5 to 3 eV (later results will show that the best film surface is produced at an incident energy of 3 eV). This again confirms that an incident energy of 0.49 eV represents some kind of an energy barrier threshold, which must be overcome if a better film surface property is to be produced.

Figure 2(c) shows the growing morphology at an incident energy of 3 eV. It will be observed that a smooth film is

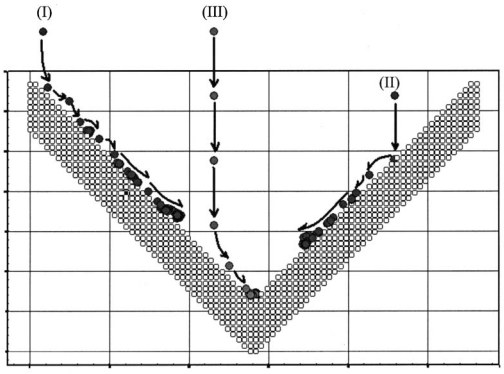

FIG. 5. Motion trace of three specific atoms deposited at three different locations for incident energy of 10 eV at initial stage of the deposition process.

produced at this level of incident energy. This indicates that an incident energy of 3 eV is sufficient to overcome the energy barrier that results in the formation of islands during deposition, and therefore the film grows in a layer-by-layer mode.

An interesting phenomenon is found when the incident energy is continuously increased to a relatively high level of 10 eV, as shown in Fig. 2(d). The deposited atoms accumulate at the bottom of the *V* groove and cause an uneven film thickness along the two inclined surfaces. The accumulation of the deposited atoms is strongly connected to the oblique deposition relative to the *V*-shape substrate as discussed as follows.

Figures 5 and 6 show the motion trace of specific atoms, selected according to their deposition position in the *y* direction, at an incident energy of 10 eV. Figure 5 considers the trace of an atom at an initial state during the deposition process, while Fig. 6 presents the trace at an intermediate state. In Fig. 5, the motion traces indicated by (I) and (II) demonstrate that the atoms deposited near the top of either inclined surface have migrated a long distance, and have approached the bottom of the *V* groove. As may be seen by motion trace (III) in Fig. 5, an atom with a deposition position located near the bottom of the *V* groove has migrated to the bottom of the groove, and has become trapped there. It is worth mentioning that the atoms jump above the substrate during the migration, as may be seen by the three motion traces in Fig. 5. The motion traces at the initial stage of the deposition process show that the deposited atoms have the tendency to approach the bottom of the *V* groove due to their high incident energy.

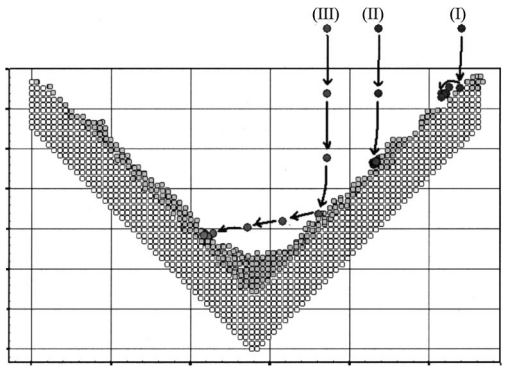

FIG. 6. Motion trace of three specific atoms deposited at three different locations for incident energy of 10 eV at intermediate stage of the deposition process.

Figure 6 shows three motion traces indicated as (I), (II), and (III), which represent the trajectory of atoms deposited at an intermediate point during the later stage of the deposition process. The motion traces represented by (I) and (II) show that the deposited atoms have become trapped by the previously deposited atoms. As would be expected, their migration distance is considerably less than the results shown in Fig. 5, which show the initial state of the process, and which therefore involve a substrate free of deposited atoms. As shown by motion trace (III) in Fig. 6, the deposited atom reflects off the substrate. It will be noted that the incident angle and the reflective angle are almost equal. Occurrence of reflection of the incident atom depends not only on the incident energy, which is considered to be the main factor for this phenomenon in Ref. 27, but also upon the surface structure. Consider, for example, a coarse surface structure, such as the cluster gathering surface. This surface type will more easily absorb the incident atom energy, and therefore the probability of atom reflection is smaller. This is the physical explanation for the phenomenon that may be observed for motion traces (I) and (II) in Fig. 6, where the deposited atoms do not reflect from the substrate. By comparison, motion trace (III) in Fig. 6 shows the case where a deposited atom hits a denser surface. On this type of surface the incident energy is less easily absorbed and thus reflection takes place. Although, the probability of deposited atoms reaching the bottom of the *V* groove is reduced during the later stages of the deposition stage due to their tendency to become trapped by previously deposited atoms on the substrate, the large incident energy of the impact still contributes slightly to an accumulation of the atoms at the bottom of the *V* groove.

The roughness of the film produced by atom deposition is characterized by its interface width. Figure 7 shows the interface width at the final steady state for different incident energies. The results indicate that a parabolic relationship exists between the interface width and the incident energy. As the incident energy initially increases, the produced film surface property improves, i.e., the interface width decreases. The figure shows that the optimal surface property is obtained when the incident energy is approximately equal to 3 eV, and that from that point on the surface property quality deteriorates as the incident energy continues to increase. This confirms that there exists an optimal value of the process parameter of incident energy, which produces the best film surface property.

2. Effect of incident angle

This part of the simulation considers the influence of incident angle variations on the deposited atoms. It provides an assessment of how the deposited film surface property may be improved by changing the deposition angle of the incident atoms.

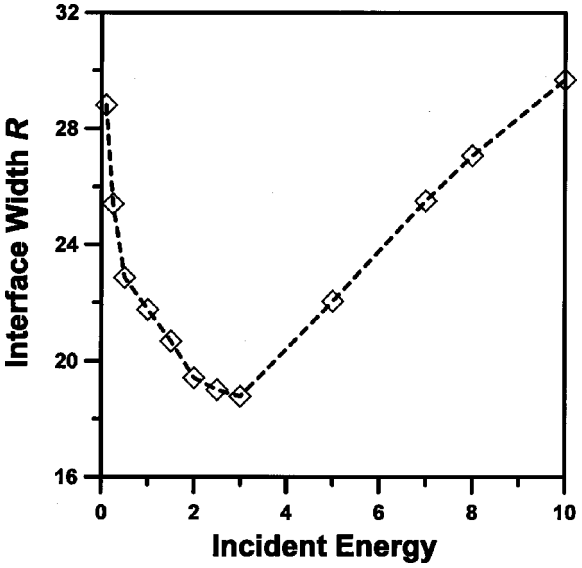

FIG. 7. Interface width at steady state for different incident energies.

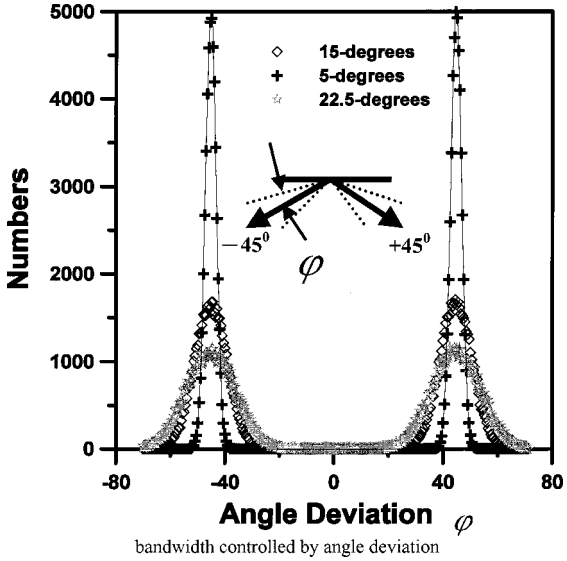

FIG. 8. Angular distributions of incident atoms of the second type; bandwidth controlled by angle deviation.

Two types of incident angle distributions are simulated: bandwidth controlled by cutoff angles and bandwidth controlled by angle deviation. The first is given by a Gaussian distribution which is restricted such that it lies within a cutoff angle. The angle distribution function varies as different cutoff angles are selected. The distribution bandwidth, whose center is located at 0°, is controlled by the cutoff angle. The simulation considers the influence of different cutoff angles, e.g., 45°, 50°, 55°, 60°, and 62.5°. The simulation of the incident angle variation reflects the practical manufacturing process where the incident angle is controlled by collimated magnetron sputter deposition. It is noted that the selection of a wide cutoff angle range, i.e., between 45° and 62.5°, will enable identification of the conditions under which the best film surface property is produced.

The second type of incident angle distribution considered is also given by a Gaussian distribution. However, in this case the main deposition angle is concentrated around two inclined directions of ±45°, as shown in Fig. 8. The maximum probability of the incident angle appearance is now located at ±45° rather than that at angle of 0° as in the previous case. The bandwidth of the angular distribution is controlled by the deviation angle from these two inclined directions. The simulation considers the following deviation angles: 5°, 10°, 15°, 20°, and 22.5°. As has been noted previously, in practice the incident angle variation can be controlled by the rotatable cylindrical magnetron system. It is to be noted that the first type of incident angle distribution is a simplified case of the second type, only one maximum probability of the incident angle appearance centered at 0°, bandwidth controlled by the deviation angles, φ, equal to half of the cutoff angle.

Figure 9 shows the interface width at final state versus the cutoff angle, at incident energies of 0.25, 5, and 10 eV. The interface widths for vertical deposition are plotted for comparison purposes, and are indicated by the solid symbols located on the vertical axis. The results indicate that there is negligible improvement in the deposited film surface property over the cutoff angle range. This may be explained by the fact that the incident angle of the majority of the deposited atoms is still located in the vertical direction of 0°. It is also observed that the values of interface width for vertical deposition are close to those of oblique deposition controlled within a cutoff angle.

Figure 10(a) shows the final deposited film morphology at an incident energy of 0.25 eV with no incident angle variation, i.e., vertical deposition. Figures 10(b)–10(d) show the final deposited film morphology at the same incident energy, but for oblique deposition with deviation angles of 5°, 15°, and 22.5°, respectively. Comparison of Fig. 10(b) with Fig. 10(a) shows that the film morphology is greatly improved by changing the incident angle to the two inclined directions of ±45°. The void tracks forming between two adjacent clus-

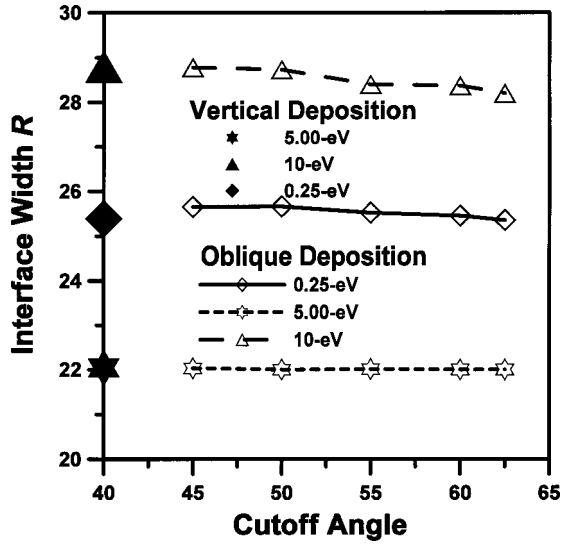

FIG. 9. Interface width at final state versus the cutoff angle at incident energies of 0.25, 5, and 10 eV.

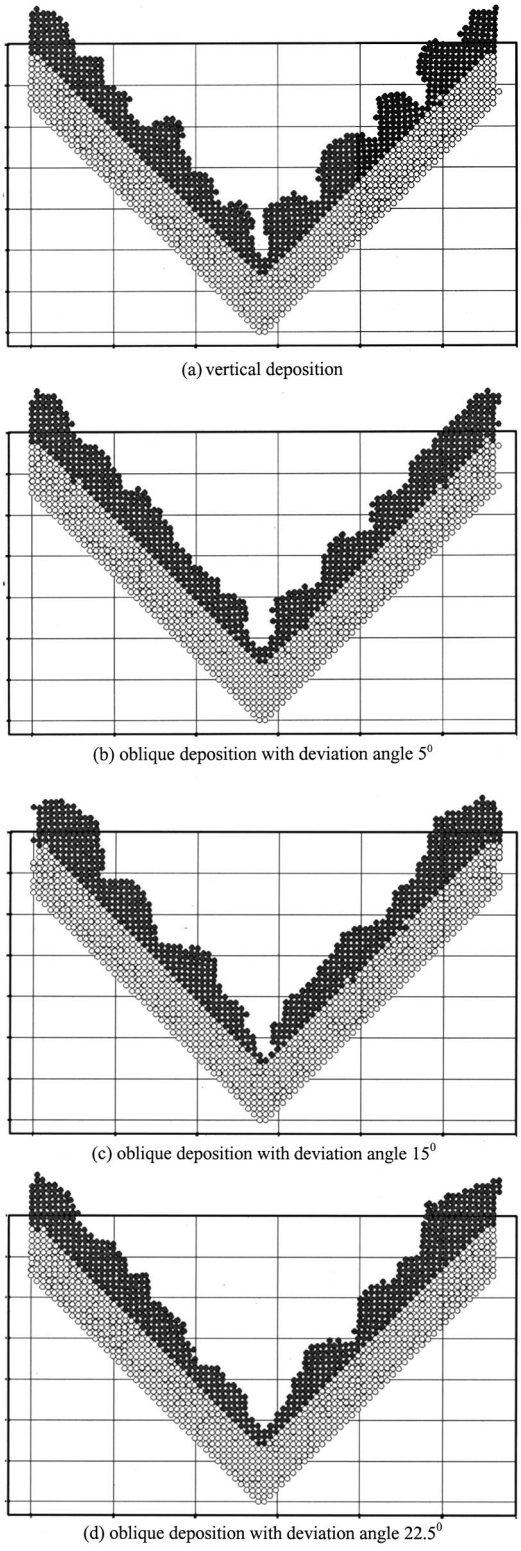

FIG. 10. Morphology of deposited film at final steady state at incident energy of 0.25 eV (a) vertical deposition, and oblique deposition with different deviation angles; (b) 5°; (c) 15°; (d) 22.5°.

ters apparently disappear. The forming of the void tracks shown in Fig. 10(a) is due to the self-shadowing mechanism[24] in which the forming clusters prevent the obliquely deposited atoms from filling the void tracks. Observation of Figs. 10(b), 10(c), and 10(d) suggests that the produced film surface property deteriorates as the deviation angle moves further and further away from the two inclined directions of $\pm 45°$. It will be noted that the void track at the bottom of the *V* groove does not significantly improve as the deviation angle increases. In direct contrast to the case of vertical deposition, the area around the bottom of the *V* groove is the location of the groove which is the most difficult to fill when using oblique deposition. The self-shadowing effect is more significant upon the filling of the bottom of the *V* groove than upon either of the two sides of the *V*-shape substrate. Any cluster formations on these sides will prevent subsequently deposited atoms from reaching the bottom of the groove.

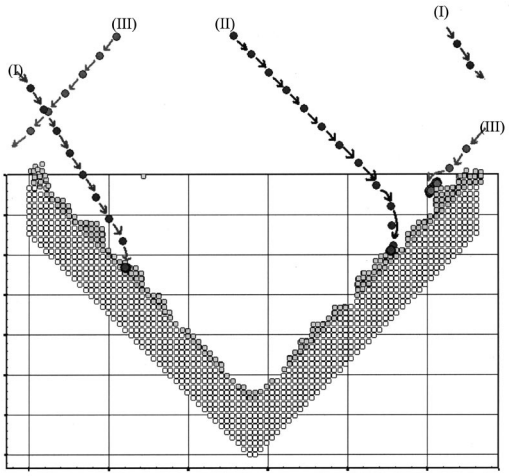

FIG. 11. Motion trace of three specific atoms deposited at incident energy of 0.25 eV with a deviation angle of 20°.

Figure 11 shows the motion traces of three specific atoms, indicated by (I), (II), and (III), at an incident energy of 0.25 eV, and with a deviation angle of 20°. Motion trace (I) considers a deposited atom whose incident angle has a bias from $+45°$. It shows that the atom is trapped by the substrate atoms. Similarly, as shown by motion trace (II) in Fig. 11, a deposited atom whose incident angle is close to $+45°$ is also trapped by the substrate atoms. From these two results, it is noted that the incident path becomes curved under the influence of the attractive force exerted by the gathering cluster. Motion trace (III) considers a deposited atom whose incident angle is close to $-45°$. It would be expected that this atom be deposited on the left side of the *V*-shape substrate. However, as may be seen in the figure, the atom is actually trapped by the cluster of atoms located at the upper part of the right side of the *V*-shape substrate. This may be explained by the attractive force that is exerted on the atom by the forming cluster. From the results presented in Fig. 11 it is possible to conclude that when the incident energy is relatively low, the motion of subsequently deposited atoms is significantly influenced by the initially grown film structure. The situation where atoms are deposited on an initially grown film with a cluster structure yields film surfaces with the worst properties. The initially forming cluster will trap more incident atoms as the deposition process continues, and will become larger. This can be seen in Fig. 10(c)

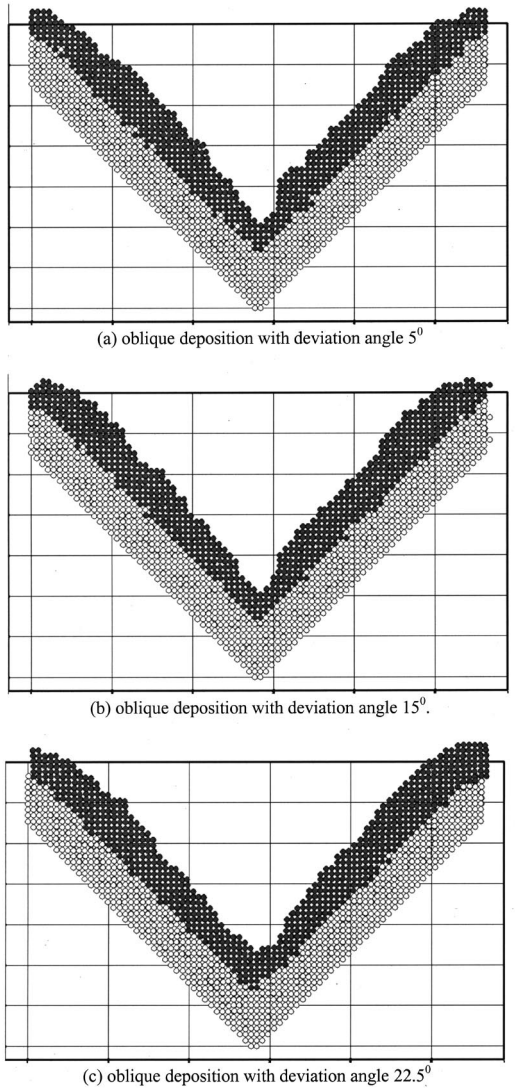

FIG. 12. Morphology of deposited film at final steady state at incident energy of 10 eV by oblique deposition with different deviation angles: (a) 5°; (b) 15°; (c) 22.5°.

on both sides of the *V* groove, and in Fig. 10(d) on the right side of the *V*-shape substrate. The forming of large clusters also induces the self-shadowing effect, which hinders the migration of deposited atoms to the bottom of the *V* groove.

Figures 12(a) to 12(c) show the final deposited film morphology with an incident energy of 10 eV at three different deviation angles of 5°, 15° and 22.5°. [The film produced by vertical deposition at this level of incident energy has already been shown in Fig. 2(d)]. The results presented in these figures indicate that the produced film morphology is greatly improved by changing the deposition angle, especially the reduction in thickness of the bulgy part at the bottom of the *V* groove.

Figure 13 shows the motion trace of three specific atoms at an incident energy of 10 eV, and with a deviation angle of 20°. Motion trace (I) indicates that the deposited atom has been resputtered[27] by the other incident atoms. Motion trace

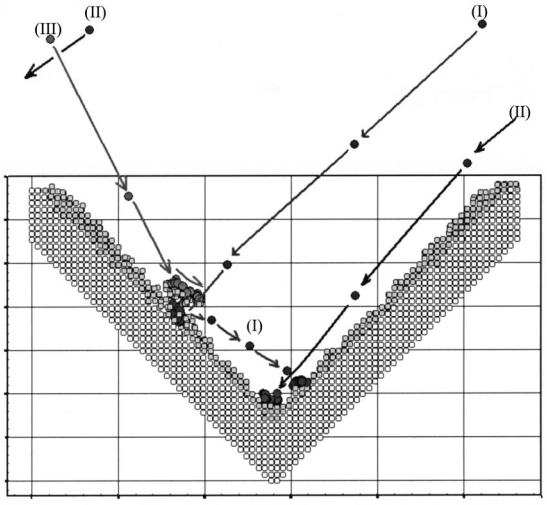

FIG. 13. Motion trace of a specific atom deposited at incident energy of 10 eV with a deviation angle of 20°.

(II) shows that the incident atom passes above the right side of the *V*-shape substrate and reaches the bottom of the *V* groove. Motion trace (III) shows the incident atom with a bias angle from +45° striking the substrate. It is noted that the reference substrate of motion trace (III) is thicker than motion traces (I) and (II), thus, only the parts of substrate atoms around the landing zone of the tracing atom are plotted. In comparison with the former results of the growing mechanism at a low incident energy of 0.25 eV, the incident path is not affected by the substrate atoms, and the deposited atom remains on its straight-line path. In addition, its travel distance is longer than when the incident energy is 0.25 eV, and this enables the incident atom to reach the bottom of the *V* groove, as indicated by motion trace (II) in Fig. 13. This is comparable to the situation shown as the motion trace (III) in Fig. 11 where an incident atom with a low incident energy of 0.25 eV is trapped by the substrate atoms. Although the flight path of the incident atoms is close to the substrate atoms in both examples, the migration distance after the incident atom has hit the substrate is longer when the incident energy is higher. This may be clearly observed by comparing the motion trace (III) in Fig. 13 with the results presented in Fig. 11. Since the migration ability of a deposited atom, and hence its ability to reach the bottom of the *V* groove, is dependent upon its incident energy, the depth of the void track for an incident energy of 10 eV is shallower than where the incident energy is 0.25 eV, as shown in Figs. 10(b) to 10(d).

Figure 14 shows the statistical result of the relationship between the interface width and the incident energy for five different deviation angles of 5°, 10°, 15°, 20°, and 22.5°. The interface width for vertical deposition is also plotted, and is indicated by the solid symbols located on the vertical axis. It has been noted previously that in general, the film surface property is improved by concentrating the deposition angle of the incident atoms around two inclined directions of ±45°. Figure 14 indicates the changes in surface property which occur for different deviation angles at three different

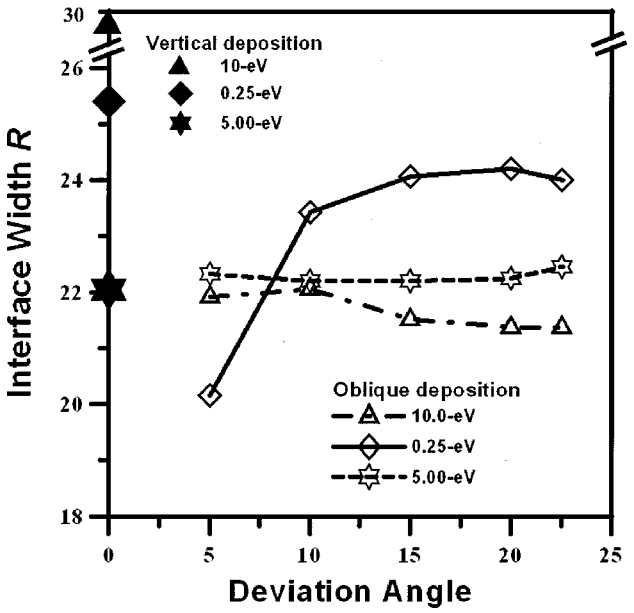

FIG. 14. Relationship of interface width to deviation angle at steady state for different incident energies.

levels of incident energy. In the case of relatively low incident energy, i.e., 0.25 eV, the film surface property deteriorates as the deviation angle from the two inclined directions of $\pm 45°$ increases. At an intermediate incident energy level of 5 eV, it is observed that there is an insignificant change in the film surface property as the incident angle is varied, and that in fact the film surface property may actually be worse than that produced by vertical deposition. Analysis of the final morphology for an incident energy of 5 eV suggests that an increase of deviation angle is slightly beneficial in reducing the depth of the void track at the bottom of the *V* groove. However, there is no improvement in the roughness of the film surface property. Compared to the results observed for relatively lower incident energy, it is found that the film surface property is greatly improved as the deviation angle increases for the high incident energy of 10 eV. From the above, it is clear that the different influences of the deviation angle on the film surface property are strongly connected to the incident energy, and should be discussed in more detail.

It has been observed that the migration ability of the incident atoms is limited when the incident atoms are deposited at a relatively low incident energy. Thus, in this case the film surface property depends strongly on the incident direction. A smaller deviation angle indicates that the deposition direction is closer to vertical deposition relative to the inclined substrate. On the other hand, as the atoms' deposition angle deviates from the two inclined directions of $\pm 45°$, the deposition tends to oblique deposition. These oblique deposition atoms influence film growth and the film tends to grow in a cluster mode. As a consequence, smaller deviation angles yield a better film surface property at relatively low incident energy.

For incident energy at a relatively high level, the migration ability of the deposited atoms becomes an important factor in determining the produced film surface property. Incident atoms with a variety of incident angles provide the highest probability of momentum transfer occurring between incident adatoms and film atoms in many directions. Thus, the momentum of the incident atoms can diffuse uniformly to the surface atoms. This is beneficial in producing superior film surface property. On the other hand, where the direction of the incident atoms is more specific, the momentum of the incident atoms diffuses less uniformly to the surface atoms. This results in the worse film surface properties observed for the smaller deviation angles.

IV. CONCLUSION

This paper has presented the use of MD simulation in investigating film growth on a GMR corrugated structure. It has been found that different growing characteristics exist for different incident energies as well as for different deposition directions, namely, vertical and oblique depositions. These include the film growing in FM, VW, and Stranski-Krastanow (SK) modes for different incident energies. Moreover, it has been observed that the incident direction also has a significant influence on the film surface property, and that this influence strongly depends upon the incident energy. Several important conclusions may be drawn from this study. These conclusions are summarized as follows.

(1) Film growth tends to be in a three-dimensional cluster mode at a relatively low incident energy. The void track forming direction is almost equal to the surface normal to the two inclined surfaces, and may be explained by the fact that the deposited Co atoms possess higher surface energy than the Cu substrate atoms.

(2) There exists an optimal incident energy that produces the best film surface property. In the case studies considered within this current study, the optimal incident energy was found to be 3 eV, which is far larger than the activation energy of the Co adatom on the fcc Co(100), i.e. 0.49 eV.

(3) The film surface property is worse when the incident energy is at a relatively high level. The uneven thickness along the *V* shape mainly arises from the deposited atoms accumulated at the bottom of the *V* groove. This accumulation may be explained by the fact that the migration distance is higher for high energy incident atoms, and therefore atoms of this type tend to approach the bottom of the *V* groove.

(4) The film surface property can be improved by changing the incident direction to two inclined directions of $\pm 45°$. A smaller deviation angle away from these two directions yields the better film surface property for small incident energy. By contrast, small deviation angles result in worse film surface property for larger incident energy.

During investigation of the growing mechanism it has been found that reflection and resputter occurs at relatively high incident energy. In addition, it has been observed that the incident path of atoms deposited at relatively low incident energy becomes curved under the influence of the resultant force exerted by the gathering cluster.

Several results obtained from the present simulation have been compared with those published previously,

and which relate to either experimental or numerical analysis. For example, the current study explains the great improvement in the film surface property as the incident energy increases to 0.5 eV, a fact noted in former experimental results. This also indicates the validity of the present study.

ACKNOWLEDGMENTS

The authors gratefully acknowledge the support given to this research project by the National Science Council, Republic of China, under Grants Nos. NSC89-2212-E-006-201 and NSC89-2218-E006-050.

*Author to whom correspondence should be addressed. Email address: weng@mail.ncku.edu.tw

†Email address: chchwang@mail.ncku.edu.tw

‡Email address: changjg@mail.ncku.edu.tw

[1] C. Tsang, R. E. Fontana, T. Lin, D. E. Heim, V. S. Speriousu, B. A. Gurney, and M. L. Williams, IEEE Trans. Magn. **30**, 3801 (1994).

[2] Hidefumi Yamamoto and Kazuhiko Yamada, Mater. Sci. Eng., B **B31**, 207 (1995).

[3] D. D. Tang, P. K. Wang, V. S. Speriousu, S. Le, and K. K. Kung, IEEE Trans. Magn. **31**, 3206 (1995).

[4] K. Matsuyama, H. Asada, S. Ikeda, and K. Taniguchi, IEEE Trans. Magn. **33**, 3283 (1997).

[5] A. S. Ebrahim, R. S. Huang, and C. T. Kowk, IEEE Electron Device Lett. **16**, 166 (1995).

[6] M. Suzuki, T. Ohwaki, and Y. Taga, Thin Solid Films **304**, 333 (1997).

[7] M. A. M. Gijs, S. K. J. Lenczowski, and J. B. Giesbers, Phys. Rev. Lett. **70**, 3343 (1993).

[8] P. M. Levy, S. Zhang, T. Ono, and T. Shinjo, Phys. Rev. B **52**, 16 049 (1995).

[9] M. Ruhrig, B. Khamsehpour, K. J. Kirk, J. N. Chapman, P. Aitchison, S. McVitie, and C. D. W. Wilkinson, IEEE Trans. Magn. **32**, 4452 (1996).

[10] S. Y. Chou, M. Wei, P. R. Krauss, and P. B. Fischer, J. Vac. Sci. Technol. B **12**, 3695 (1994).

[11] I. Nakatani, IEEE Trans. Magn. **32**, 4448 (1996).

[12] E. E. Fullerton, D. M. Kelly, J. Guimpel, J. K. Schuller, and Y. Bruynseraede, Phys. Rev. Lett. **68**, 895 (1992).

[13] H. Ueda, O. Kitakami, Y. Shimada, Y. Goto, and M. Yamamoto, Jpn. J. Appl. Phys. **33**, 6173 (1994).

[14] Boquan Li, Honglie Shen, Yoshiyuki Saitoh, Toshiyuki Fujimoto, and Isao Kojima, Thin Solid Films **315**, 104 (1998).

[15] M. El Harfaoui, H. Le Gall, J. Ben Youssef, S. Pogossian, A. Thiaville, P. Gogol, A. Qachaou, and J. M. Desvignes, J. Magn. Magn. Mater. **198-199**, 107 (1999).

[16] Y. Saito, S. Hashimoto, and K. Inomata, Appl. Phys. Lett. **60**, 2436 (1992).

[17] R. J. Highmore, W. C. Shih, R. E. Somekh, and J. E. Evetts, J. Magn. Magn. Mater. **116**, 249 (1992).

[18] M. A. M. Gijs, M. T. Johnson, A. Reinders, P. E. Huisman, R. J. M. van de Veerdonk, S. K. J. Lenczowski, and R. M. J. van Gansewinkel, Appl. Phys. Lett. **66**, 1839 (1995).

[19] G. A. Bird, *Molecular Gas Dynamic and the Direct Simulation of Gas Flows* (Oxford University Press, New York, 1994).

[20] J. W. Evans, D. E. Sanders, P. A. Thiel, and A. E. DePristo, Phys. Rev. B **41**, 5410 (1989).

[21] R. W. Smith and D. J. Srolovitz, J. Appl. Phys. **79**, 1448 (1996).

[22] C. L. Kelchner and A. E. DePristo, Nanostruct. Mater. **8**, 253 (1997).

[23] A. Robbemond and B. J. Thijsse, Nucl. Instrum. Methods Phys. Res. B **127-128**, 273 (1997).

[24] L. Dong, R. W. Smith, and D. J. Srolovitz, J. Appl. Phys. **80**, 5682 (1996).

[25] X. W. Zhou, R. A. Johnson, and H. N. G. Wadley, Acta Mater. **45**, 1513 (1997).

[26] S. P. Ju, C. I. Weng, J. G. Chang, and C. C. Hwang, J. Appl. Phys. **89**, 7825 (2001).

[27] X. W. Zhou and H. N. G. Wadly, Surf. Sci. **431**, 58 (1999).

[28] F. Cleri and V. Rosato, Phys. Rev. B **48**, 22 (1993).

[29] V. Rosato, M. Guillope, and B. Legrand, Philos. Mag. A **59**, 321 (1989).

[30] I. Meunier, G. Treglia, B. Legrand, R. Tetot, B. Aufray, and J.-M. Gay, Appl. Surf. Sci. **162-163**, 219 (2000).

[31] F. Hontinfinde, R. Ferrando, and A. C. Levi, Surf. Sci. **366**, 306 (1996).

[32] A. Belkind, W. Gerristead, Jr., and Z. Orban, Thin Solid Films **207**, 319 (1992).

[33] G. Mazzone, V. Rosato, and M. Pintore, Phys. Rev. B **55**, 837 (1997).

[34] J. M. Haile, *Molecular Dynamic Simulation* (Wiley, New York, 1992).

[35] J. W. Evans, D. E. Sanders, P. A. Thiel, and A. E. DePristo, Phys. Rev. B **41**, 5410 (1989).

[36] M. T. Kief and W. F. Egelhoff, Jr., Phys. Rev. B **47**, 10 785 (1993).